Science
AAAS

Geodynamo, Solar Wind, and Magnetopause 3.4 to 3.45 Billion Years Ago

John A. Tarduno, *et al.*

Science **327**, 1238 (2010);
DOI: 10.1126/science.1183445

Geodynamo, Solar Wind, and Magnetopause 3.4 to 3.45 Billion Years Ago

John A. Tarduno,[1,2]* Rory D. Cottrell,[1] Michael K. Watkeys,[3] Axel Hofmann,[3] Pavel V. Doubrovine,[1,4] Eric E. Mamajek,[2] Dunji Liu,[5] David G. Sibeck,[6] Levi P. Neukirch,[2] Yoichi Usui[1,7]

Stellar wind standoff by a planetary magnetic field prevents atmospheric erosion and water loss. Although the early Earth retained its water and atmosphere, and thus evolved as a habitable planet, little is known about Earth's magnetic field strength during that time. We report paleointensity results from single silicate crystals bearing magnetic inclusions that record a geodynamo 3.4 to 3.45 billion years ago. The measured field strength is ~50 to 70% that of the present-day field. When combined with a greater Paleoarchean solar wind pressure, the paleofield strength data suggest steady-state magnetopause standoff distances of ≤5 Earth radii, similar to values observed during recent coronal mass ejection events. The data also suggest lower-latitude aurora and increases in polar cap area, as well as heating, expansion, and volatile loss from the exosphere that would have affected long-term atmospheric composition.

The oldest record of Earth's magnetic field strength, based on a thermoremanent magnetization (TRM), is from silicate crystals hosting single domain–like magnetite inclusions separated from plutons from the Kaapvaal craton, South Africa; these plutons have been dated to 3.2 billion years ago (Ga) (*1*). This record suggests an intensity that is within 50% of the modern field value. The geomagnetic field may be truly ancient, starting shortly after core formation, but several hypotheses suggest otherwise. A null or weak field at 3.8 to 3.9 Ga is predicted from a hypothesis seeking to explain lunar nitrogen values through transport from Earth's atmosphere by the solar wind (*2*). A delayed onset of the geodynamo, to ages as young as 4.0 to 3.4 Ga, has been predicted from a model for cooling of a dense liquid layer at the base of the early Earth's magma ocean (*3*). However, testing these null-field models is difficult because of the ubiquitous metamorphism that has affected Paleoarchean terrestrial rocks.

Some of the least metamorphosed Paleoarchean rocks, having experienced peak temperatures of <350°C [e.g., (*4*)], are found in the Barberton Greenstone Belt (BGB) in South Africa. Chemical remagnetization associated with Fe mobilization during metamorphism is also a concern. Paleomagnetic and rock magnetic studies suggest that some dacitic rocks of the BGB have largely escaped this problem, probably because of a relatively low Fe content. Specifically, dacite clasts pass a conglomerate test, indicating magnetization prior to 3.42 Ga (*5*). The ~3.45-Ga dacite parent body for the clasts, however, reveals a high–unblocking temperature magnetization with scatter greater than that seen in younger rocks. The simplest explanation for the large dispersion of magnetic directions is the presence of multidomain magnetic grains in the dacite, seen in thin section (*5*), that are susceptible to carrying magnetic overprints. Alternatively, the scatter could reflect magnetization in the absence of a geodynamo, in a field related to solar wind interaction with the atmosphere. A good discriminator of external versus internal terrestrial fields is paleointensity. Using modern Venus as an example of a planet lacking a dynamo (*6*), we expect that solar wind–atmosphere interaction will create a field that is highly variable in direction and at least an order of magnitude weaker than the post–3.2 Ga dynamo-driven field recorded on Earth.

We tested the nondynamo magnetization scenario by sampling dacites from two Kaapvaal craton localities for paleointensity analysis: the Hooggenoeg Formation in the BGB (*7*) and the Witkop Formation in the Nondweni Greenstone Belt (NGB) (*8*, *9*); the latter is located ~300 km south of the BGB. Several authors have reported ages of ~3.445 Ga for the BGB dacite (*5*, *10*), whereas new SHRIMP Pb-Pb zircon data reported here (*10*) (fig. S1 and table S1) indicate an age of 3.409 ± 0.004 Ga for the NGB dacite site used in our study. The BGB dacite is a shallowly emplaced body that likely once linked to extrusive (now eroded) counterparts. Our samples were collected within 1 km of the contact with the overlying Buck Reef Chert (*7*), but the dacite body appears to represent the accumulation of many smaller intrusions. We assume that our BGB site represents a sample of one of these 100- to 200-m-thick intrusive events. The NGB site is from a flow or very shallow sill that is 100 m thick where sampled. Hand samples were collected from topographic lows of exposures of both dacites to avoid the effects of modern lightning strikes. A field test for the age of remanence similar to that reported for the BGB dacite (*5*) is unavailable for our NGB site, but the high–unblocking temperature in situ magnetic direction seen in whole rock samples is far removed from later overprint directions (fig. S2).

Single silicate crystals can host magnetic carriers with single domain–like behavior, avoiding complexities posed by the presence of multidomain grains [e.g., (*11*, *12*)]. We isolated quartz phenocrysts, 0.5 to 2 mm in size, as oriented and unoriented samples. Preparation and selection followed prior studies (*1*, *13*) and included the provision that samples could not show visible inclusions under low magnification, thereby excluding samples with larger multidomain magnetic inclusions. This required a search through hundreds of BGB crystals; the NGB dacites, however, yielded cleaner quartz crystals suitable for paleomagnetic and rock magnetic measurements.

Magnetic hysteresis data measured with an alternating gradient force magnetometer (Princeton Measurements Corp.) confirmed the presence of single-domain to pseudo–single-domain carriers in the quartz crystals, whereas whole rocks clearly contained multidomain contributions (fig. S3). Thellier-Coe paleointensity measurements were carried out on unoriented crystals, using both heating with a thermal demagnetization oven and a CO_2 laser (*10*). Natural remanent magnetizations (NRMs) were measured with a 2G DC 755R superconducting quantum interference device (SQUID) magnetometer with high-resolution sensing coils or with a new 2G DC SQUID magnetometer with a small (diameter 6.3 mm) room-temperature access bore optimized for single-crystal studies. Demagnetization data showed the removal of one or more components at unblocking temperatures less than ~450°C; this agrees with theory predicting the temperature range where an overprint acquired under low-grade metamorphism should contaminate the magnetization (*14*). At higher unblocking temperatures, the magnetization showed univectorial decay and linear NRM/TRM characteristics (Fig. 1), with maximum unblocking characteristics consistent with a magnetite carrier. Paleointensity data that met acceptance criteria (*10*, *15*) (tables S2 and S3) were available from 12 BGB and seven NGB quartz crystals; these yield average field intensities of 28.0 ± 4.3 and 18.2 ± 1.8 μT, respectively. The paleointensity values showed strengths that are unexpected from magnetization mechanisms in the absence of a geodynamo [e.g., (*5*)]. Thus, these data extend the record of a geodynamo back in time 250 million years, from 3.2 (*1*) to ~3.45 Ga.

We applied the thin-section technique to obtain oriented quartz crystals (*13*) from NGB samples, yielding a paleoinclination of –42.4° ± 5.9° (n = 7; table S4). Only two samples prepared from BGB dacite thin sections met the selection

[1]Department of Earth and Environmental Sciences, University of Rochester, Rochester, NY 14627, USA. [2]Department of Physics and Astronomy, University of Rochester, Rochester, NY 14627, USA. [3]School of Geological Sciences, University of KwaZulu-Natal, Durban 4000, South Africa. [4]Physics of Geological Processes, University of Oslo, Oslo 0316, Norway. [5]Beijing SHRIMP Centre, Chinese Academy of Geological Sciences, 26 Baiwanzhuang Road, Beijing 100037, China. [6]Code 674, NASA/Goddard Space Flight Center, Greenbelt, MD 20771, USA. [7]Department of Earth Sciences, Tohoku University, Sendai, Miyagi 980-8578, Japan.

*To whom correspondence should be addressed. E-mail: john@earth.rochester.edu

criteria (*10*). Nonetheless, analyses of these samples (table S4) suggest a paleoinclination (–44.5° ± 11.1°) similar to that of the NGB dacite, which implies that the two greenstone belts formed in close proximity. Paleolatitude data (*1*) from 3.2-Ga BGB rocks (~29°), when compared to the NGB (~25°) and BGB (~26°) data, yield a minimum long-term plate velocity of <1 cm/year, hinting at the slow rates suggested by some models of mantle cooling (*16*). When referenced to these paleolatitudes, the paleointensity data suggest a virtual dipole moment (VDM) of 3.8 (±0.4) × 10^{22} A m^2 for the NGB dacite and 5.8 (±0.9) × 10^{22} A m^2 for our BGB site, corresponding to 48 and 73% of the modern value, respectively.

Unlike paleointensity estimates from 3.2-Ga plutons of the Kaapvaal craton (*1*), which cooled over tens of millions of years, our paleointensity data should be less affected by cooling rates because of the relatively shallow (or surface) emplacement of the dacites. The cooling time (*17*) to reach 450°C, the approximate starting point of our paleointensity data calculations, is ~30 years for the NGB dacite and ~90 to ~400 years for our BGB sample site (*10*).

If the magnetic inclusions are adequately represented by some theoretical considerations of cooling rate effects on single-domain particles (*18*), our paleointensity estimates could overestimate the true paleointensity by 26 to 35% (*10*) (table S5). However, our magnetic hysteresis data point toward grains having single-domain to pseudo–single-domain characteristics; micromagnetic modeling suggests that the latter will slightly underestimate field strength if they are locked in a vortex state on geological time scales and blocked in the single-domain state in the laboratory (*19*). The net effect of these contrasting cooling rate effects is probably small. Although the shallow emplacement of the dacites lessens the potential influence of cooling rates on paleointensity values relative to more deeply emplaced rocks [e.g., (*1*)], it also implies that the units record less time. A potential limitation of the VDMs, therefore, is that they represent field averages only over decades (NGB) and centuries (BGB).

We next examined the implications of our paleointensity data with respect to shielding of radiation from the young Sun. We again used the dipole assumption because this maximizes the magnetic shielding (*20*) and hence provides a conservative estimate of conditions at ≥3.4 Ga. The magnetopause standoff distance (r_s) at the subsolar point is determined by the balance of the solar wind pressure and Earth's magnetic field (*21*)

$$r_s = \left[\frac{\mu_0^2 f_0^2 M_E^2}{4\pi^2(2\mu_0 P_{sw} + B_{IMF}^2)}\right]^{1/6} \quad (1)$$

where M_E is Earth's dipole moment, P_{sw} is solar wind ram pressure, f_0 is a magnetospheric form factor (= 1.16 for Earth), μ_0 is the permeability of free space, and B_{IMF} is the interplanetary magnetic field; contributions from the latter are minor. We used two approaches to assess the ancient solar wind. Changes in solar wind ram pressure can be related to changes in mass loss rate ($\dot{m}$) and solar wind velocity (v_{sw}) [e.g., (*22*, *23*)]. Studies of young solar analogs (*23*) suggest a power-law mass loss from which we can derive a relationship between current (t_0, P_{sw0}, $\dot{m}_0$, v_{sw0}) and past values

$$\frac{P_{sw}}{P_{sw0}} = \frac{\dot{m} v_{sw}}{\dot{m}_0 v_{sw0}} = \left(\frac{t}{t_0}\right)^{-2.33} \quad (2)$$

This suggests a mass loss at 3.45 Ga of 2.4 × 10^{-13} $M_\odot$/year, where $M_\odot$ is the present solar mass. In the resulting model A (*10*), wind pressure change with time leads to estimates of magnetopause standoff distance as a function of dipole moment (Fig. 2). Our paleointensity estimates at ≥3.4 Ga suggest a considerable decrease of the standoff distance, to between 45 and 51% of the present 10.7 Earth radii (R_E). The solar wind pressure changes (Fig. 2) also imply that standoff reductions are robust on a time scale of millions to tens of millions of years, assuming that our paleointensity values sample secular variation broadly similar to that of the younger geomagnetic field (*10*).

In another approach, we started with stellar evolution models and predicted that the Sun at 3.45 Ga would appear to be a G6V star with a rotational period of ~12 days (*10*, *24*). Mass loss rates among solar-type stars correlate with x-ray

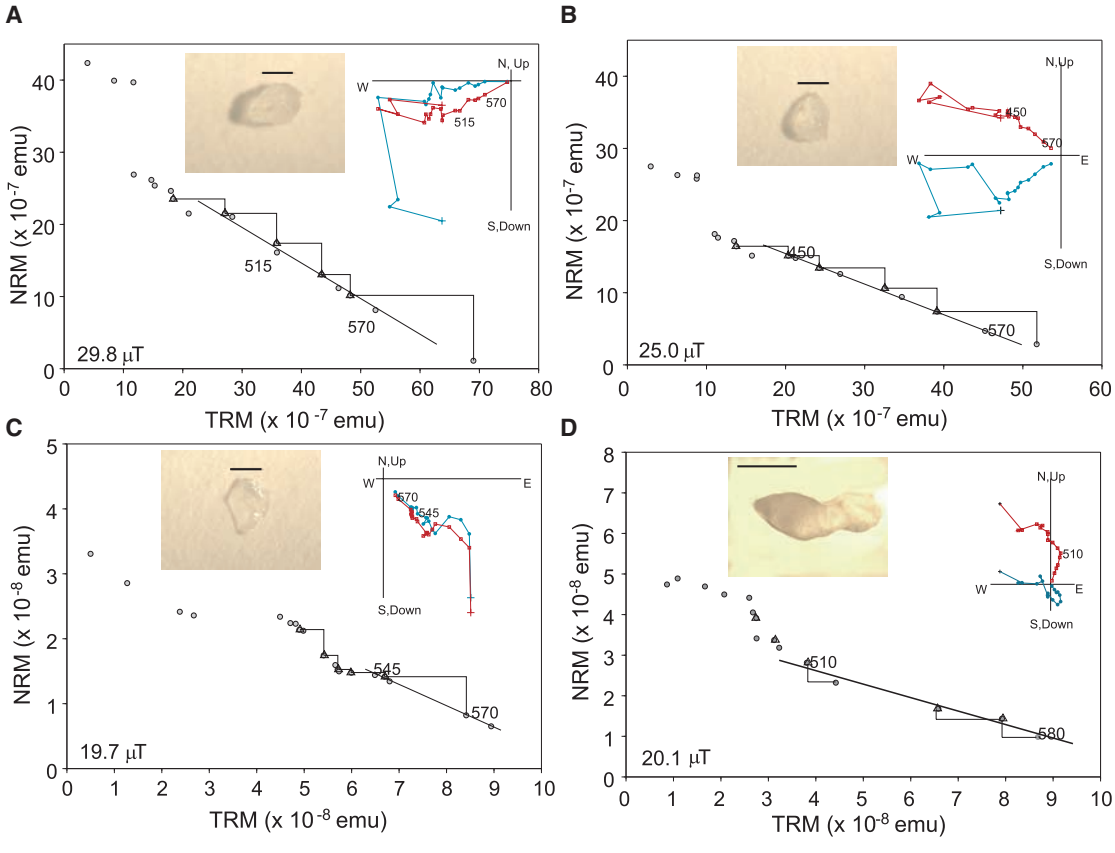

Fig. 1. Paleointensity data examples. For each panel, inset image shows crystal as measured (scale bar, 1 mm); inset at upper right is orthogonal vector plot of field-off magnetization (red, inclination; blue, declination; unoriented samples shown). Main panels are plots of natural remanent magnetization (NRM) versus thermal magnetization (TRM); plotted values are circles, with partial TRM checks shown as triangles (*10*). Line fit shows data used for paleointensity calculation (numerical value at lower left). (**A** and **B**) Examples from Barberton Greenstone Belt locality, using thermal demagnetization oven heating. (**C**) Example from Nondweni Greenstone Belt, using thermal demagnetization oven heating. (**D**) Example from Nondweni Greenstone Belt, using CO_2 laser heating (*1*) of grain from oriented thin section in geographic coordinates.

emission (f_X), which in turn correlates with rotation. We estimated mass loss as

$$\dot{m} = \dot{M}_\odot \left(\frac{R}{R_\odot}\right)^2 \left(\frac{f_X}{f_{X_\odot}}\right)^{1.34\pm0.18} \quad (3)$$

where R is solar radius, $R_\odot$ is the modern value, and $f_{X_\odot}$ is the modern soft x-ray surface flux. This yields a higher mass loss of 1.5×10^{-12} $M_\odot$/year (model B) and an even smaller standoff distance, between 3.6 and 4.2 R_E. The reductions in standoff distance are similar to (model A) or greater than (model B) those characterizing extreme modern events, such as the Halloween solar storm of 2003 [e.g., (*25*)]. However, these standoffs would have been typical, rather than the exceptional day-long deviations associated with modern coronal mass ejections (CMEs).

The continuous Halloween storm conditions would have resulted in aurora at far lower latitudes than is typically the case today. We used a scaling law derived from the pressure balance between the solar wind and Earth's magnetic field (*26*) to determine the latitude of the aurora, namely the location of the polar cap boundary dividing closed (~dipolar) magnetospheric magnetic field lines from open lines that extend into the magnetotail and thence into interplanetary space:

$$\cos(\lambda_p) = \left(\frac{M_E}{M_{E_0}}\right)^{-1/6} P^{1/12} \cos(\lambda_{p_o}) \quad (4)$$

where λ_p is the magnetic latitude of the polar cap edge, λ_{p_o} is the present value (71.9°), M_{E_0} is the present dipole moment, and P is the solar wind dynamic pressure normalized to its present value of ~2 nPa. This scaling relationship suggests that at 3.4 to 3.45 Ga, the area of the polar cap increased up to a factor of 3 (model B) relative to the present, allowing solar energetic particles far greater access to Earth's atmosphere.

The smaller standoff distances and larger polar cap area would result in heating and expansion of Earth's exosphere, promoting loss of volatiles and water (*27*). An early, high loss rate of hydrogen may have been an important factor in the transition from a mildly reducing to an oxidizing atmosphere (*28*), whereas an early, high loss rate of water implies that Earth had a greater initial water inventory. We also note that whereas our estimates make use of time-averaged estimates of solar wind pressures, Sun-like stars with ages of ~1 Ga are observed to have more frequent and energetic x-ray flares than those of the current Sun (*29*). Presumably, CMEs would also have been more frequent and energetic. Individual CMEs could decrease standoff to levels much less than time-averaged values, exacerbating any impact on the exosphere. Thus, although a Paleoarchean geodynamo produced a magnetic field that would have prevented whole-scale atmospheric erosion, magnetic field and solar wind strengths suggest important modifications during the first billion years of Earth evolution. The dynamo suggested by our paleointensity data is near the oldest age suggested for inner core growth (*30*). More extensive changes in the atmosphere and Earth's water budget would have occurred if an earlier dynamo driven solely by thermal convection was weaker, or if dynamo action was delayed (*2*, *3*).

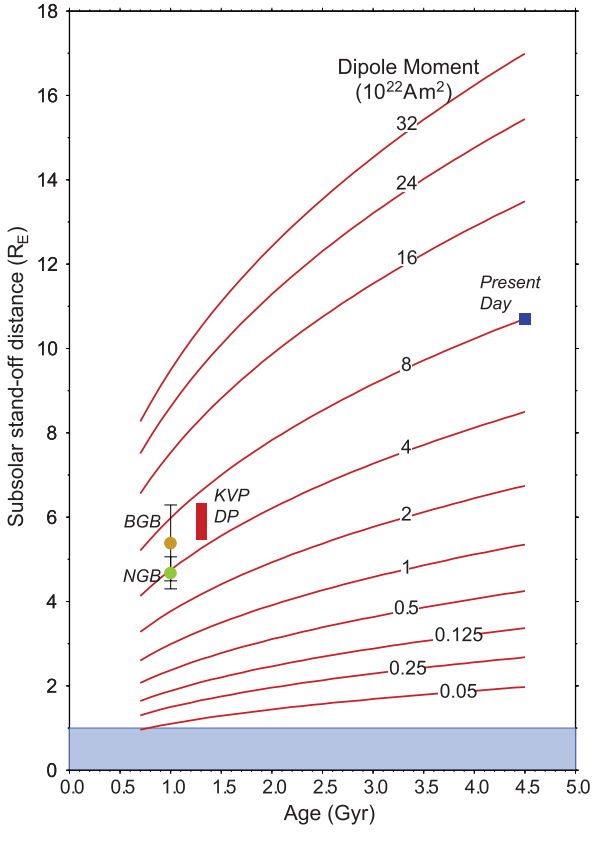

Fig. 2. Subsolar magnetopause standoff distance (expressed in Earth radii) versus dipole moment with respect to the age of Earth (in billions of years), with present-day value (blue square) and estimates from 3.2-Ga Kaap Valley (KVP) and Dalmein plutons (DP) [range from values uncorrected to corrected for cooling rate assuming single-domain behavior shown (*1*)] and virtual dipole moments from the Barberton Greenstone Belt (BGB) and Nondweni Greenstone Belt (NGB) dacite localities.

References and Notes

1. J. A. Tarduno, R. D. Cottrell, M. K. Watkeys, D. Bauch, *Nature* **446**, 657 (2007).
2. M. Ozima *et al.*, *Nature* **436**, 655 (2005).
3. S. Labrosse, J. W. Hernlund, N. Coltice, *Nature* **450**, 866 (2007).
4. M. M. Tice, B. C. Bostick, D. R. Lowe, *Geology* **32**, 37 (2004).
5. Y. Usui, J. A. Tarduno, M. K. Watkeys, A. Hofmann, R. D. Cottrell, *Geochem. Geophys. Geosyst.* **10**, Q09Z07 (2009).
6. T. L. Zhang *et al.*, *Nature* **450**, 654 (2007).
7. D. R. Lowe, G. R. Byerly, *Geol. Soc. Am. Spec. Pap. 329* (1999).
8. A. H. Wilson, J. A. Versfeld, *Precambrian Res.* **67**, 243 (1994).
9. A. Hofmann, A. H. Wilson, in *Earth's Oldest Rocks*, M. J. Van Kranendonk, R. H. Smithies, V. C. Bennett, Eds. (Elsevier, Amsterdam, 2007), pp. 571–605.
10. See supporting material on *Science* Online.
11. R. D. Cottrell, J. A. Tarduno, *Earth Planet. Sci. Lett.* **169**, 1 (1999).
12. J. M. Feinberg, G. R. Scott, P. R. Renne, H. R. Wenk, *Geology* **33**, 513 (2005).
13. J. A. Tarduno, R. D. Cottrell, A. V. Smirnov, *Rev. Geophys.* **44**, RG1002 (2006).
14. D. J. Dunlop, K. L. Buchan, *Phys. Earth Planet. Inter.* **13**, 325 (1977).
15. R. D. Cottrell, J. A. Tarduno, *J. Geophys. Res.* **105**, 23579 (2000).
16. J. Korenaga, *Rev. Geophys.* **46**, RG2007 (2008).
17. J. C. Jaeger, in *Basalts: The Poldervaart Treatise on Rocks of Basaltic Composition*, H. H. Hess, A. Poldevaart, Eds. (Wiley-Interscience, New York, 1967), vol. 2, pp. 503–536.
18. S. E. Halgedahl, R. Day, M. Fuller, *J. Geophys. Res.* **85**, 3690 (1980).
19. M. Winklhofer, K. Fabian, F. Heider, *J. Geophys. Res.* **102**, 22695 (1997).
20. G. L. Siscoe, D. G. Sibeck, *J. Geophys. Res.* **85**, 3549 (1980).
21. J.-M. Grießmeier *et al.*, *Astron. Astrophys.* **425**, 753 (2004).
22. G. Newkirk Jr., *Geochim. Cosmochim. Acta Suppl.* **13**, 293 (1980).
23. B. E. Wood, *Space Sci. Rev.* **126**, 3 (2006).
24. E. E. Mamajek, L. A. Hillenbrand, *Astrophys. J.* **687**, 1264 (2008).
25. L. Rosenqvist *et al.*, *J. Geophys. Res.* **110**, A09S23 (2005).
26. G. L. Siscoe, C.-K. Chen, *J. Geophys. Res.* **80**, 4675 (1975).
27. Y. N. Kulikov *et al.*, *Space Sci. Rev.* **129**, 207 (2007).
28. H. Lammer *et al.*, *Space Sci. Rev.* **139**, 399 (2008).
29. A. Telleschi *et al.*, *Astrophys. J.* **622**, 653 (2005).
30. D. Gubbins, D. Alfe, G. Masters, G. D. Price, M. Gillan, *Geophys. J. Int.* **157**, 1407 (2004).

31. We are grateful to the late William Goree for his encouragement and design of the small-bore SQUID magnetometer and to the staffs of William Goree Inc. and Applied Physics for final construction of the instrument. We thank J. Hopkins for assistance in the laboratory and G. Kloc for sample preparation. Supported by NSF grants EAR 0738844 and EAR 0619467 and the John Simon Guggenheim Foundation (J.A.T.).

Supporting Online Material

www.sciencemag.org/cgi/content/full/327/5970/1238/DC1
Materials and Methods
Figs. S1 to S3
Tables S1 to S5
References

16 October 2009; accepted 15 January 2010
10.1126/science.1183445